Electrical and thermal conductivities of rare-earth $A_2Zr_2O_7$ (A = Pr, Nd, Sm, Gd, and Er)

A. Quiroz[a], V. García-Vázquez[b], C. Guarneros Aguilar[c], R. Agustín-Serrano[d], E. Chavira[e], and M. Abatal[f,*]

[a]*Universidad Tecnológica de Xicotepec de Juárez, Área Mantenimiento Industrial y Petróleo. Av. Universidad Tecnológica No. 1000, Col. Tierra Negra, C.P. 73080, Cd. Xicotepec de Juárez, Pue., Mexico, adolfo.quiroz@utxicotepec.edu.mx*

[b]*Instituto de Física Luis Rivera Terrazas, Benemérita Universidad Autónoma de Puebla, Apartado Postal J-48, Puebla, Pue., 72570, Mexico; e-mail: lema@ifuap.buap.mx*

[c]*CONACYT- Instituto Politécnico Nacional, Materiales y Tecnologías para Energía Salud y Medio Ambiente (GESMAT), CICATA Altamira, Km 14.5 Carretera Tampico-Puerto Industrial Altamira, 89600, Altamira, Tamaulipas, Mexico, e-mail: cguarnerosagag@conacyt.mx*

[d]*Facultad de Ciencias Físico Matemáticas, Benemérita Universidad Autónoma de Puebla, Av. San Claudio y 18 Sur, Ciudad Universitaria, Puebla, Pue. 72570 Mexico, e-mail: ricardo.agustion@correo.buap.mx*

[e]*Instituto de Investigaciones en Materiales, Universidad Nacional Autónoma de México, Apartado Postal 70-360 Ciudad de Mexico, 04510 Mexico, e-mail: chavira@unam.mx*

[f]*Facultad de Ingeniería Universidad Autónoma del Carmen, Av. Central S/N Esq. con Fracc. Mundo Maya, Ciudad del Carmen, Campeche, 24115 Mexico.*

[*]*e-mail: mabatal@pampano.unacar.mx; Tel.: (+0052 938 38 11018, ext.: 1700-1703)*

Received 19 August 2020; accepted 22 September 2020

Structural and thermoelectric properties of rare-earth zirconates $A_2Zr_2O_7$, with A = Pr, Nd, Sm, Gd, and Er, were studied. Samples were prepared by solid-state reaction at ambient pressure with temperatures between 1000 and 1400 °C. The resulting compounds were characterized by X-ray diffraction (XRD) and scanning electron microscopy (SEM/EDS). The XRD analyses showed the formation of polycrystalline Pr_2Zr_2O7, $Nd_2Zr_2O_7$, $Sm_2Zr_2O_7$, $Gd_2Zr_2O_7$, and $Er_2Zr_2O_7$ phases, with a cubic cell (space group Fm3m) and traces of the raw used materials. The micrographs obtained by SEM show the formation of heterogeneous grains with a size that ranges from 0.7 to 4.7 μm. All $A_2Zr_2O_7$ samples present porous surfaces. Thermal conductivities were measured at different temperatures, from 300 to 900 K. In most of the samples, the thermal conductivity monotonically decreases with temperature, from 0.40 - 1.17 W/mK at 300 K to 0.27 - 0.77 W/mK at 773.15 K. At a fixed temperature, the thermal conductivity decreases almost monotonically with the ionic radius (IR) of the rare-earth elements (where IR (Er^{3+}) = 0.890 Å $< IR$ (Gd^{3+}) = 0.938 Å $< IR$ (Sm^{3+}) = 0.958 Å $< IR$ (Nd^{3+}) = 0.983 Å $< IR$ (Pr^{3+}) = 0.99 Å).

Keywords: Solid state chemistry; thermal analysis; X-ray diffraction and scattering; thermoelectrics; zirconates.

PACS: 82.33.Pt; 61.05.cp; 77.70.+a; 72.20.Jv

DOI: https://doi.org/10.31349/RevMexFis.67.255

1. Introduction

In the past decades, there has been a significant interest in thermoelectric (TE) materials study. These materials are characterized by their capability to convert waste heat into electricity. Achieving a high-energy conversion efficiency in TE materials, however, has been the major obstacle for cost-effective applications [1-7]. The conversion efficiency of material for TE applications is characterized in terms of the dimensionless figure of merit ZT of the TE material, $ZT = \alpha 2\sigma T/\kappa$, where α is the Seebeck coefficient, σ the electrical conductivity, T the operation temperature, and κ the total thermal conductivity (lattice and electronic contributions) [5,6]. Therefore, it becomes interesting to investigate the thermoelectric properties of compounds that already have low thermal conductivity.

One family of compounds that might satisfy such requirements is the rare-earth zirconates. With a chemical formula $A_2Zr_2O_7$ (A = rare-earth element), these materials are ceramics that present either an ordered pyrochlore-type structure or a defective fluorite-type phase since the structure has a different formula than the fluorite structure $(A,Zr)_4O_8$ [7-9]. The rare-earth zirconates show interesting thermophysical properties. They present thermal and chemical stability, low thermal conductivity, and high thermal expansion, among other characteristics [10]. These promising attributes allow the rare-earth zirconates to consider them excellent candidates for different industrial application, such as thermoelectric devices, thermal barrier coatings (TBCs), environment barrier coatings, etc. [11].

In order to consider rare-earth zirconates, or any other

compound, as good prospects for thermoelectric applications, they must satisfy specific characteristics in their thermoelectric performance. The materials must have high electrical conductivity (from 0.01 to 0.6 S/cm), a high Seebeck coefficient (from 130 to 225 μV/K), and low thermal conductivity (from 0.5 to 0.75 W/mK) [12-15]. One of the important properties of the rare-earth zirconates that might offer a better figure of merit ZT is their low thermal conductivity. Thermal conductivities in these compounds have been reported to be considerably lower than the characteristic values obtained in yttria-stabilized zirconia [16-22], a compound commonly used in current TBC. Since the electrical and thermal conductivity values of the pyrochlorides, as well as the Seebeck coefficient, depend on the experimental conditions such as temperature and reaction time, as well as the concentration and type of the doped ion [14,23,24], it results interesting to explore further these compounds.

Pyrochlore oxides, in general, have been considered as promising candidates as solid-oxide fuel cell cathodes. The cationic disorder in these compounds favors the Frenkel-defect formation responsible for the high-ionic conductivity and the oxide-ion diffusion in these materials [25,26]. In addition to the general properties of the Pyrochlore oxides and the particular characteristics of the rare-earth zirconates presented above to make such unexplored materials a promising alternative as possible cathodes in fuel cells.

In this paper, we investigate the thermoelectric properties of rare-earth zirconates. We are interested in obtaining polycrystalline $A_2Zr_2O_7$ compounds with A = Pr, Nd, Sm, Gd, and Er via the solid-state reaction method. In particular, we study the heat-thermal conditions during sample preparation for which the compounds can be obtained. Electrical and thermal conductivities, as well as Seebeck coefficients, are determined as a function of temperature. We report the relationship between the structural and thermoelectric properties of the $A_2Zr_2O_7$ compounds.

2. Materials and methods

2.1. Synthesis by solid-state reaction

Polycrystalline $A_2Zr_2O_7$ samples (A = Pr, Nd, Sm, Gd, and Er) were synthesized by solid-state reaction. Before the reaction, the purity of the starting materials ZrO_2 (Riedel-de Haën, 99.9%), Pr_2O_3 (Aldrich, 99.9 %), Nd_2O_3 (Cerac, 99.9 %), Sm_2O_3 (Aldrich, 99.9%), Gd_2O_3 (Aldrich, 99.9%), and Er_2O_3 (Aldrich, 99.9%) was verified by X-ray powder diffraction (XRD). The stoichiometric amounts of reagents were mixed and ground in an agate mortar for 30 min in order to get a homogeneous powder [27]. The resultant $A_2Zr_2O_7$ powders were compressed into pellets (13 mm diameter, $1.0 - 1.5 \pm 0.05$ mm thickness) by applying a pressure of 3 tons/cm^2 for 5 minutes under vacuum. After that, the pellets were heated in the air from room temperature up to 1400°C at 10°C/min, kept at 1400°C for 72 h, and then cooled down to room temperature at 3°C/min.

2.2. Characterization techniques

Thermogravimetric analysis (TGA) was performed in order to study the thermal behavior of each $A_2Zr_2O_7$ compound. The analyses were carried out by using TA Instruments SDT Q600 equipment, from 25 to 1200°C. XRD measurements were performed on an APD 2000 diffractometer with Cu$K\alpha$ radiation ($\lambda = 1.5406$ Å) and a graphite monochromator. The XRD patterns were obtained at ambient temperature from 10° to 90° with a step size of 0.025° and a time per step of 15 sec. Rietveld refinement of the XRD patterns was performed by using the MAUD refinement software [28]. This program was developed by Wenk *et al.* [29] and Ferrari and Lutterotti [30] to analyze diffraction data in order to obtain the crystal structures of the samples.

Sample morphology and grain size were characterized by scanning electron microscopy (SEM) by using a Hitachi S-3400N-II system equipped with an EDAX 9900 device that permits to determine the chemical composition of the samples by energy-dispersive X-ray spectrometry (EDS/EDX).

For the thermoelectric characterization, square-shaped compacts ($10 \times 10 \times 0.5$ mm) were prepared by using a 3-ton hydraulic press. Seebeck coefficient and electric conductivity were simultaneously measured in a high-precision SBA 458 Nemesis Netzsch system. Measurements were performed from 300 to 900 K under a 10 sscm N2 flux and applying a current of 0.05 A. The heater voltage for Seebeck measurements was 1.0 V, whereas the temperature increment and the temperature difference threshold were 5 K/s and 15 K, respectively. Thermal conductivity was measured on a LFA 467 HyperFlash Netzsch system equipped with a xenon flash lamp and an InSb detector. Experiments were also performed from 300 to 900 K, with a pulsed energy up to 10 J/pulse and a pulse width of $20 - 1200$ μs.

3. Results and discussions

3.1. Thermal analysis

Previous to the synthesis process, the $A_2Zr_2O_7$ compounds were examined by thermogravimetric analysis (TGA) to determine the temperatures at which the formation of subproducts takes place during the solid-state reaction process. The TGA curves of the samples are shown in Fig. 1. To simplify, the TGA thermograms are divided into three relevant regions according to the following reaction temperatures: $25 - 200$°C, $200 - 800$°C, and $800 - 1200$°C.

In the first region, a weight loss of 0.05 - 2.95% was observed in the $Sm_2Zr_2O_7$ and $Er_2Zr_2O_7$, $Nd_2Zr_2O_7$, and $Gd_2Zr_2O_7$ samples, respectively. This result can be attributed to the humidity and possible water condensation on the samples' surfaces. For the $Pr_2Zr_2O_7$ sample, a gain of 0.09% was obtained, which can be explained by the possible reaction of the sample surface with the surrounding atmosphere.

In the second region, the $Pr_2Zr_2O_7$ sample exhibits around 0.15% of mass gain, which can be attributed to a pos-

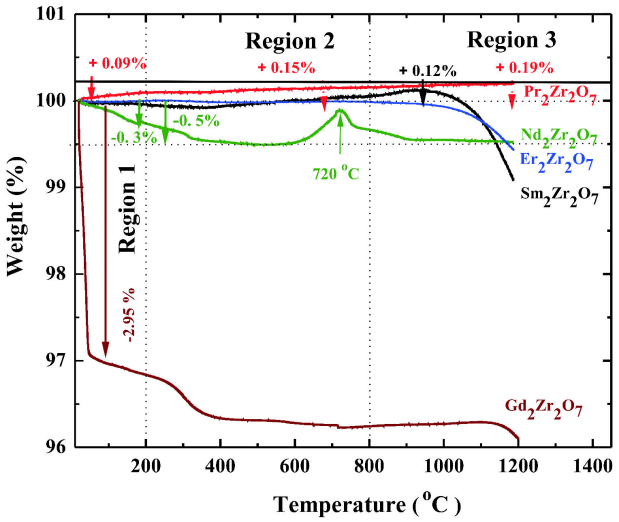

FIGURE 1. Thermogravimetric curves of the $Pr_2Zr_2O_7$, $Nd_2Zr_2O_7$, $Er_2Zr_2O_7$, $Sm_2Zr_2O_7$, and $Gd_2Zr_2O_7$ samples.

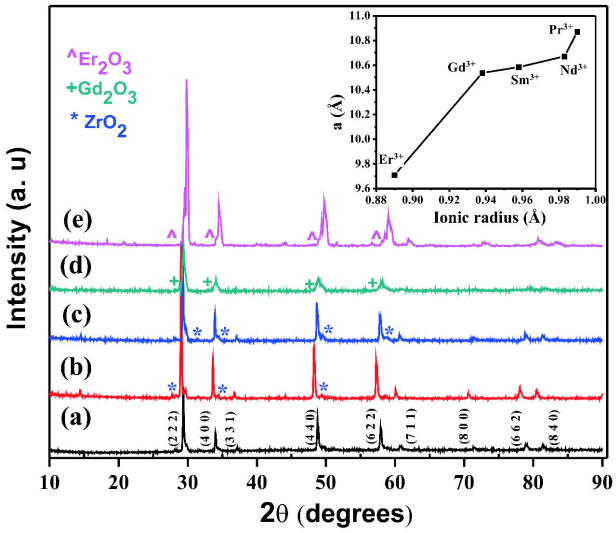

FIGURE 2. XDR patterns of the $A_2Zr_2O_7$ samples sintered at 1400°C. a) $Pr_2Zr_2O_7$. b) $Nd_2Zr_2O_7$. c) $Sm_2Zr_2O_7$. d) $Gd_2Zr_2O_7$. e) $Er_2Zr_2O_7$. Inset: Cell parameter a as a function of the ionic radius.

sible reaction with the surrounding atmosphere [31], whereas a negligible variation in weight was observed for the $Pr_2Zr_2O_7$ and $Sm_2Zr_2O_7$ samples. For the $Nd_2Zr_2O_7$ and $Gd_2Zr_2O_7$ samples, 0.5 and 3.5% of their weight loss, respectively, was detected between 200 and 400°C. This can be related to possible oxidation caused by the decomposition at higher temperatures. Between 600 and 800°C, a mass gain was obtained as a consequence of the reaction of the $Nd_2Zr_2O_7$ sample with the atmosphere at 720°C.

In the third stage, below 1000°C, the TGA results show a mass gain of 0.12 and 0.19% for the $Sm_2Zr_2O_7$ and $Er_2Zr_2O_7$ samples, respectively. Above 1000°C, no weight loss is presented in the $Nd_2Zr_2O_7$ and $Pr_2Zr_2O_7$ samples, which prove the elimination of all products before the formation of the desired compound.

3.2. Crystalline strucrure and phase composition

The XRD patterns of the $A_2Zr_2O_7$ samples (A = Pr, Nd, Sm, Gd, and Er) are shown in Fig. 2. The results indicate the formation of Pyrochlore-type cubic phase with Fd3m space group (S.G. number 227). Main diffraction peaks, such as (222), (400), (331), (440), (662), (711), (800, and (662), and (840), are found in all samples. These peaks originate from the pyrochlorate structure [23-32,33]. Other minor peaks corresponding to raw materials were detected in some samples, such as ZrO_2 (S.G. P21/a, no.14), Gd_2O_3 (S.G. I_{a3}, no.206), and Er_2O_3 (S.G. Fm-3m, no. 225) [34], indicating that minor quantity of reagents was not reacted.

The XRD patterns of the rare-earth samples were refined by using the MAUD software program [28]. The results showed a good agreement with the experimental pattern, confirming that the main phase presented in the samples is the cubic $A_2Zr_2O_7$ phase. The values of Sig and Rwp after the refinement of the XRD patterns were within $1.35 - 3.23$ and $6.184 - 23.868$, respectively. Figure 3 shows the Maud refinement of the XRD data corresponding to the $Gd_2Zr_2O_7$ sample.

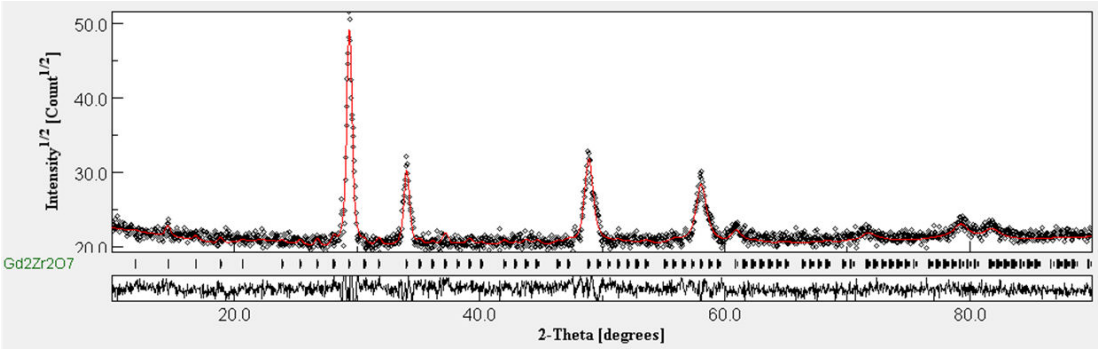

FIGURE 3. XDR patterns of the $A_2Zr_2O_7$ samples sintered at 1400°C. a) $Pr_2Zr_2O_7$. b) $Nd_2Zr_2O_7$. c) $Sm_2Zr_2O_7$. d) $Gd_2Zr_2O_7$. e) $Er_2Zr_2O_7$. Inset: Cell parameter A as a function of the ionic radius.

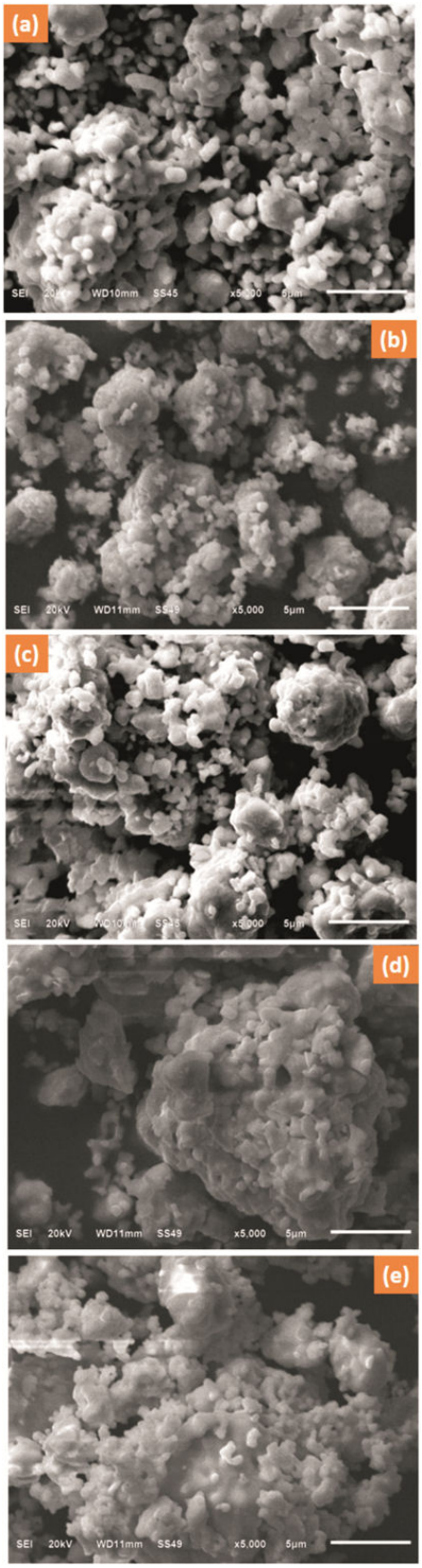

FIGURE 4. Micrographs of the a) $Pr_2Zr_2O_7$, b) $Nd_2Zr_2O_7$, c) $Sm_2Zr_2O_7$, d) $Gd_2Zr_2O_7$, and e) $Er_2Zr_2O_7$ compounds prepared at 1400°C.

The unit cell parameter A of the samples was calculated through structure Rietveld refinement. The inset of Fig. 2 shows the variation of the cubic cell parameter A as a function of the ionic radius (IR) of the rare-earth elements. An increase in the unit cell with an increase in IR of the rare-earth elements (IR(Er^{3+}) = 0.890 Å $< IR$(Gd3+) $= 0.938$ Å $< IR$(Sm^{3+}) $= 0.958$ Å $< IR$(Nd^{3+})$= 0.983$ Å$< IR$(Pr^{3+}) $= 0.99$ Å [35]) indicates the successful incorporation of the rare-earth cations into the cubic structure durin the solid-state reaction.

3.3. Morphology and chemical composition

SEM micrographs of the samples heated at 1400°C are shown in Fig. 4. The $Pr_2Zr_2O_7$, $Nd_2Zr_2O_7$, and Sm2Zr2O7 compounds show the formation of microcrystals with a size that varies between 0.7 and 2.4 μm. Moreover, it can be observed that the form of some grains are well defined, while all others form agglomerations (Figs. 4a), 4b), and 4c)).

In the $Gd_2Zr_2O_7$ and $Er_2Zr_2O_7$ samples, the grains have sizes between 0.7 and 4.7 μm [Figs. 4d), and 4e), respectively]. Our results are consistent with the work given by Lucuta *et al*. [37], where they attribute these values to the high temperature used during the synthesis. Also, it can be observed in the figures that all samples are porous. Furthermore, the pores seem to accumulate at the grain boundaries. As indicated in other works, both porosity and grain size are considered important parameters that have a significant effect on the ferroelectric properties of the ceramics samples [14-16,36,37].

3.4. Thermolectric properties

The temperature dependence of the Seebeck coefficient S of each $A_2Zr_2O_7$ compound (A = Er, Gd, Sm, Nd, and Pr) is presented in Fig. 5a). Positive and negative values of S are observed in the measured temperature interval, indicating that both conduction carriers, holes and electrons, are involved in the transport processes. Between 372 and 673 K, the absolute values of S are quite low in all samples. At temperatures higher than 673 K, the Seebeck coefficients of the $Nd_2Zr_2O_7$, $Sm_2Zr_2O_7$, and $Pr_2Zr_2O_7$ samples slightly increase as temperature increases, indicating the semiconducting nature of these rare-earth zirconates. In the $Nd_2Zr_2O_7$ sample, however, a maximum is observed at 773 K, followed by a drop. In contrast, S is kept almost constant for the $Er_2Zr_2O_7$ sample. Figure 5b) shows the values of S extracted from Fig. 5a) at the fixed temperature of 773 K. This graph permits us to appreciate better that there exists a dependence of S on the ionic radius of the rare-earth elements A. This result is consistent with the work given by Moon *et al*. [16], where it was reported that S not only depends on A but also on the degree of structural distortion that determines the electronic localization-delocalization transition.

Figure 6 shows the electrical conductivity as a function of temperature. Low values of electrical conductivity are ob-

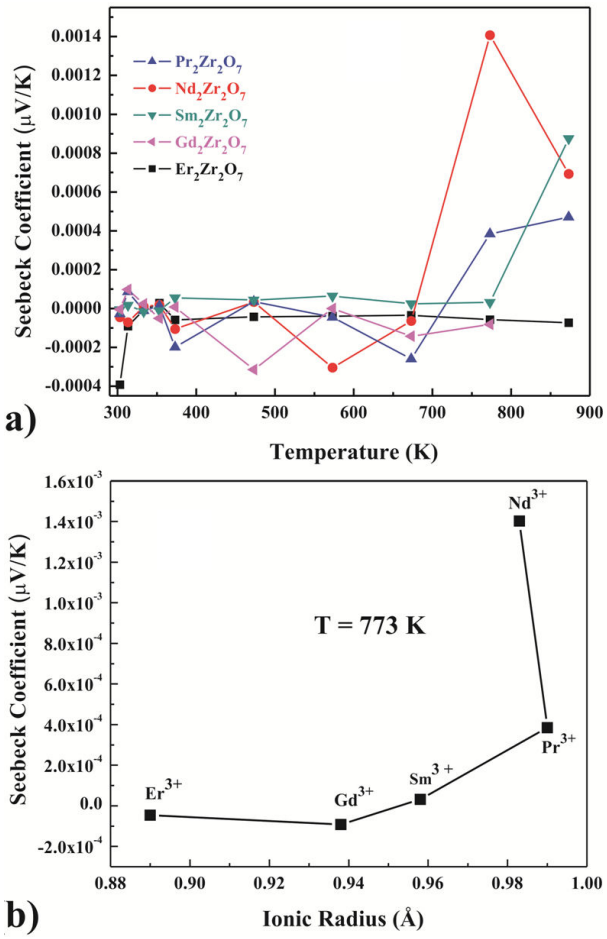

FIGURE 5. a) Seebeck coefficient of the $A_2Zr_2O_7$ compounds (A = Er, Gd, Sm, Nd, Pr) vs. temperature. b) Dependence of the Seebeck coefficient on the ionic radius of the rare-earth elements at 773 K.

served in all samples at temperatures larger than 400 K. This result can be attributed to the imperfections given by the high porosity observed in the SEM images (see Fig. 4) and to the

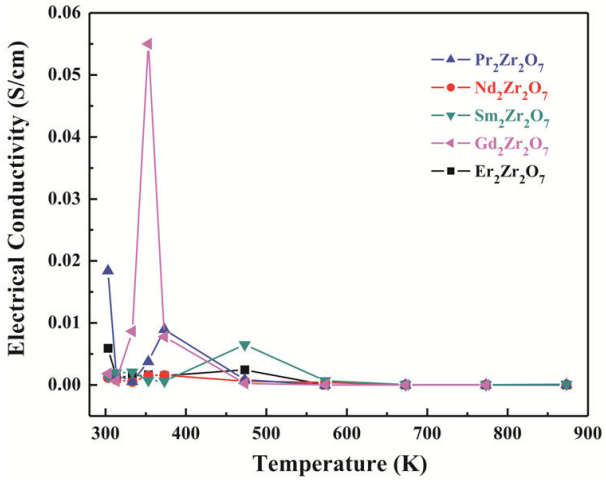

FIGURE 6. Electrical conductivity as a function of temperature for the $A_2Zr_2O_7$ compounds (A = Pr, Nd, Sm, Gd, Er).

structural disorder commonly presented in these materials [15]. In addition, it is well known that the electrical conductivity decreases with the number of charge carriers due to the filling of the valence band as a consequence of the doping. Besides, the additional electrons that are provided by the substitutional rare-earth solute cations (Pr^{3+}, Nd^{3+}, Sm^{3+}, Gd^{3+}, and Er^{3+}) and replace the zirconium (Zr^{4+}) sites are expected to shift the Fermi level from the valence band toward the middle of the bandgap [38]. It is also expected that the larger radius ratio (Pr > Nd > Sm > Gd > Er) produces higher defect-formation energy [39-41] that resist the structural transformations in the different compounds, giving rise to a low electrical conductivity.

Figure 7a) shows the temperature dependence of the thermal conductivity. Besides the $Gd_2Zr_2O_7$ sample, the thermal conductivity of all samples monotonically decreases with temperature. For the $Er_2Zr_2O_7$ sample, the thermal conducti-

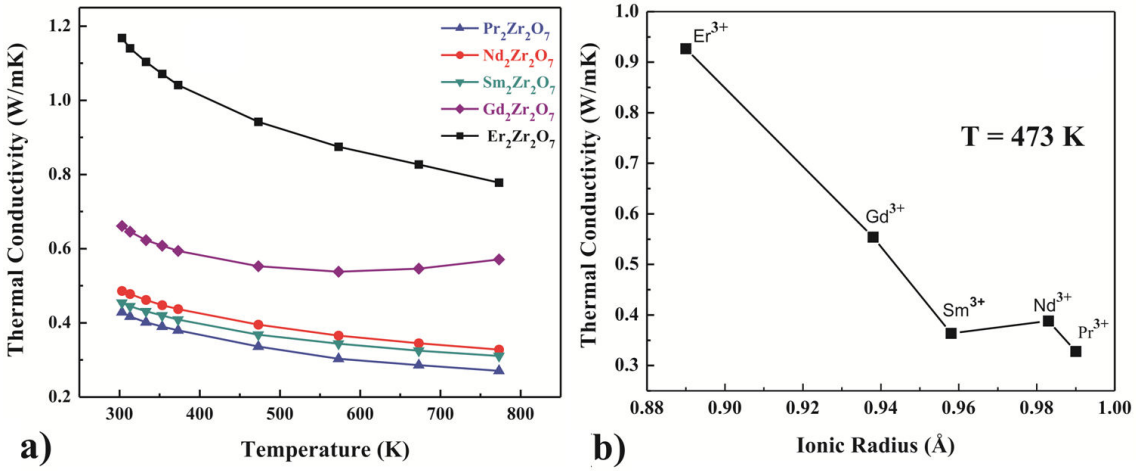

FIGURE 7. a) Thermal conductivity against temperature for the $A_2Zr_2O_7$ compounds (A = Er, Gd, Sm, Nd, Pr). b) Dependence of the thermal conductivity on the ionic radius of the rare-earth elements at 473 K.

vity goes from nearly 1.2 W/mK at 300 K to 0.8 W/mK at 773 K. For the remaining samples, lower values of the thermal conductivity are obtained. Similar results were reported by Jie and collaborators [23], where the decrease in temperature of the thermal conductivity could be associated with the improvement in the efficiency of the thermal barrier coating compounds [23,24-42]. Figure 7b) shows the values of the thermal conductivity extracted from Fig. 7a) at the fixed temperature of 473 K. A dependence of the thermal conductivity on the ionic radius of the rare-earth elements A in $A_2Zr_2O_7$ is clearly observed in the graph. A nearly monotonical behavior is obtained. The largest value of the thermal conductivity is obtained in the $Er_2Zr_2O_7$ sample, the rare-earth zirconate with the total substitutional solute cation that has the lowest ionic radius, Er^{3+}, whereas the lowest value is obtained in the sample with the largest ionic radius, Pr^{3+}.

4. Conclusions

In summary, the thermoelectric properties of rare-earth zirconates $A_2Zr_2O_7$, prepared by solid-state reaction with A = Pr, Nd, Sm, Gd, and Er, were studied. Once the samples were sintered at 1400°Cduring 72 h, the XRD analyses showed the formation of polycrystalline $Pr_2Zr_2O_7$, $Nd_2Zr_2O_7$, $Sm_2Zr_2O_7$, $Gd_2Zr_2O_7$, and $Er_2Zr_2O_7$ phases, respectively, with a cubic cell (space group Fm3m) and traces of raw materials. The chemical composition of each sintered sample, obtained by energy dispersive X-ray spectrometry (EDS/EDX) analysis, confirmed the formation of the respective desired stoichiometry with a small remaining quantity of the starting materials. Scanning electron microscopy (SEM) showed that all $A_2Zr_2O_7$ samples present porous surfaces.

The Seebeck coefficient S measured at different temperatures in all $A_2Zr_2O_7$ samples showed positive and negative values, indicating that both conduction carriers, holes and electrons, are involved in the transport processes in these rare-earth zirconates. At fixed temperatures, it was found that S increases with increasing the radius of the rare-earth ions A in the $A_2Zr_2O_7$ compounds. The electrical conductivity, measured in the same temperature interval, showed low values in all $A_2Zr_2O_7$ samples and was attributed to the imperfections given by the high porosity observed in the SEM images. Most interesting resulted from the thermal conductivity measurements. First, in most of the samples, the thermal conductivity monotonically decreased with temperature, where the $Er_2Zr_2O_7$ sample showed the largest values and the $Pr_2Zr_2O_7$ sample showed the lowest value. Second, it was found that the thermal conductivity decreases almost monotonically with the ionic radius of the rare-earth elements A in the $A_2Zr_2O_7$ samples.

All these results indicate that rare-earth zirconates could be good candidates for thermoelectric applications. The substitutional rare-earth solute cations A in $A_2Zr_2O_7$ could be used as a tuning parameter. More studies in these compounds, however, must be performed, particularly those on conversion efficiency. Besides the results suggest that rare-earth zirconates could be used as a promising alternative for cathodes in solid-oxide fuel cells.

Author Contributions

The authors contributed to the synthesis and the characterization of the materials, like the data analysis. All authors discussed the results and contributed on the final manuscript.

Acknowledgments

The authors acknowledge Engineer Karla Eriseth Reyes Morales, from IIM-UNAM, for performing TGA measurements and Juan Jesús Reyes for Seebeck coefficient and thermal conductivity measurements. The SBA 458 Nemesis and the LFA 467 HyperFlash Netszch systems were acquired by Project No. 252705 from CONACYT INFR-2015-01.

1. G. J. Snyder, M. Christensen, E. Nishibori, T. Caillat, B. B. Iversen, Disordered Zinc in Zn4Sb3 with Phonon-Glass and Electron- Crystal Thermoelectric Properties. *Nat. Mater*. **3** (2004) 458. https://doi.org/10.1038/nmat1154
2. K. F. Hsu, Cubic AgPbmSbTe2+m: Bulk Thermoelectric Materials with High Figure of Merit. *Science* **303** (2004) 818. DOI:10.1126/science.1092963
3. J. P. Heremans, Enhancement of Thermoelectric Efficiency in PbTe by Distortion of the Electronic Density of States. *Science* **321** (2008) 554. DOI:10.1126/science.1159725
4. B. C. Sales, D. Mandrus, R. K. Williams, Filled Skutterudite Antimonides: A New Class of Thermoelectric Materials. *Science* **272** (1996) 1325. DOI:10.1126/science.272.5266.1325
5. J. R. Sootsman, D. Y. Chung, and M. G. Kanatzidis, New and Old Concepts in Thermoelectric Materials. *Angew. Chem., Int. Ed.* **48** (2009) 8616. https://doi.org/10.1002/anie.200900598
6. G. S. Nolas, J. Sharp, and J. Goldsmid, *Thermoelectrics: Basic Principles and New Materials Developments*; Springer Science & Business Media: Berlin, (Germany, 2013); Vol. 45.
7. G. J. Snyder and E. S. Toberer, *Complex Thermoelectric Materials. Nat. Mater*. **7** (2008) 105. https://doi.org/10.1038/nmat2090
8. D. J. M. Bevan, Summerville, E. Mixed Rare Earth Oxides; in *Handbook on the Physics and Chemistry of Rare Earths*: Non-Metallic Compounds I. Edited by K. A. Gschneider and L. R. Eyring. North-Holland Physics Publishing, (New York. 1979); pp. 412-515.
9. M. A. Subramanian, and A. W. Sleight, Rare Earth Pyrochlores;

in *Handbook on the Physics and Chemistry of Rare Earths*. Edited by K. A. Gschneider and L. Erying. Elsevier Science Publishers, (Oxford, U.K. 1993); pp. 225-48.

10. K. Shimamura, T. Arima, K. Idemitsu, and Y. Inagaki, Thermophysical Properties of Rare-Earth-Stabilize Zirconia and Zirconate Pyrochlores as Surrogates for Actinide-Doped Zirconia. *Int. J. Thermophys.* **28** (2007) 1074. https://doi.org/10.1007/s10765-007-0232-9
11. K. Ren, Q. Wang, G. Shao, X. Zhao, and Y. Wang, Multicomponent high-entropy zirconates with comprehensive properties for advanced thermal barrier coating. *Scr. Mater.* **178** (2020) 382. https://doi.org/10.1016/j.scriptamat.2019.12.006
12. S.Y. Kim, G.E Lee, I.H. Kim, Thermoelectric Properties of Mechanically-Alloyed and Hot-Pressed Cu12-x Cox Sb4S13 Tetrahedrites. *J. Korean Phy. Soc*. **74** (2019) 967. https://doi.org/10.3938/jkps.74.967
13. C.G. Aguilar, C.E. Moreno, M.P. Castillo, F. Caballero-Briones, Effect of calcination temperature on structure and thermoelectric properties of CuAlO2 powders *J. Mater. Sci*. **53** (2018) 1646. https://doi.org/10.1007/s10853-017-1602-8
14. K. Park, K.Y. Ko, W.-S. Seo, Thermoelectric properties of CuAlO2. *J. Eur. Ceram. Soc.* **25** (2005) 2219. https://doi.org/10.1016/j.jeurceramsoc.2005.03.034
15. W. D. Kingery, H. K. Bowen, and D. R. Uhlmann, *Introduction to Ceramics* (2nd ed.). John Wiley & Sons, (New York, 1976), p. 519.
16. J.W. Moon, W.S. Seo, H. Okabe, T. Okawa, and K. Koumoto, Ca-doped RCoO3 (R = Gd, Sm, Nd, Pr) as thermoelectric materials. *J. Mater. Chem.* **10** (2000) 2007. https://doi.org/10.1039/B003964K
17. R. Vassen, X. Cao, F. Tietz, D. Basu, D. Stoever, Zirconates as New Materials for Thermal Barrier Coatings. *J. Am. Ceram. Soc.* **83** (2000) 2023. https://doi.org/10.1111/j.1151-2916.2000.tb01506.x
18. M. J. Maloney, *Thermal Barrier Coatings Systems and Materials*. U.S. Pat. 2 (000), No. 6, 117.
19. M. J. Maloney, *Thermal Barrier Coating Systems and Materials*. U.S. Pat. (2001), No. 6, 284.
20. R. Subramanian, *Thermal Barrier Coating Having High Phase Stability*. U.S. Pat. (2001), No. 6, 258.
21. G. Suresh, G. Seenivasan, M. V. Krishnaiah, and P. S. Murti, Investigation of the Thermal Conductivity of Selected Compounds of Gadolinium and Lanthanum. *J. Nucl. Mater.* **249** (1997) 259. https://doi.org/10.1016/S0022-3115(97)00235-3
22. G. Suresh, G. Seenivasan, M. V. Krishnaiah, and P. S. Murti, Investigation of the Thermal Conductivity of Selected Compounds of Lanthanum, Samarium and Europium. *J. Alloys Compd.* **269** (1998) L9. https://doi.org/10.1016/S0022-3115(97)00235-3
23. W. Jie, *et al*,. Low-Thermal-Conductivity Rare-Earth Zirconates for Potential Thermal-Barrier-Coating Applications. *J. Am. Ceram. Soc.* **85** (2002) 3031. https://doi.org/10.1111/j.1151-2916.2002.tb00574.x
24. L. Zhan-Guo, J-H. Ouyang, Y. Zhou, L. Jing, and X. Xiao-Liang, (Ln0.9Gd0.05Yb0.05)2Zr2O7 Ceramics with Pyrochlore Structure as Thermal Barrier Oxides. *Adv. Eng. Mater.* **8** (2010) 754. https://doi.org/10.1002/adem.200800079
25. E. Kendrick, J. E. Sansom, J. R. Tolchard, J. R. Islam, and P. R. Slater, Neutron diffraction and atomistic simulation studies of Mg doped apatite-type oxide ion conductors. *Faraday. Discuss.* **134** (2007) 181. https://doi.org/10.1039/B602258H
26. J. E. H. Sansom, A. Najib, and P. R. Slater, Oxide ion conductivity in mixed Si/Ge-based apatite-type systems. *Solid. State. Ion.* **175** (2004) 353. https://doi.org/10.1016/j.ssi.2003.12.030
27. A. Quiroz, E. Chavira, V. Garcia-Vazquez, G. González, M. Abatal, Structural, electrical and magnetic properties of the pyrochlorate Er2-xSrxRu2O7 ($0 \leq x \leq 0.10$) system. *Rev. Mex. Fis.* **64** (2018) 222.
28. L. Lutterotti, MAUD, Int. Union of Crystallography CPD Newsletter (IUCr), No. 24. (2000)
29. H.-R. Wenk, S. Matthies and L. Lutterotti, Texture analysis from diffraction spectra, *Mater. Sci. Forum*, **473** (1994) 157. https://doi.org/10.4028/www.scientific.net/MSF.157-162.473
30. M. Ferrari, and L. Lutterotti, Method for the simultaneous determination of anisotropic residual stresses and texture by x-ray diffraction. *J. Appl. Phys*. **76** (1994) 7246. https://doi.org/10.1063/1.358006
31. Y., Zhang, D. E. Mack, M. O. Jarligo, X. Cao, R. Vaben, and D. Stöver, Partial evaporation of strontium zirconate during atmospheric plasma spraying. J. Therm. Spray. Tech. **184** (2009) 694. https://doi.org/10.1007/s11666-009-9360-z
32. Yige Wang, Bo Gao, Qian Wang, Xiaohui Li, Zhi Su, and Aimin Chang. A2Zr2O7 (A = Nd, Sm, Gd, Yb) zirconate ceramics with pyrochlore-type structure for high-temperature negative temperature coefficient thermistor. *J Mater Sci Ceramics*. **55** (2020) 15405. https://doi.org/10.1007/s10853-020-05104-5
33. V. V. Popov, *et al.*, Comparative analysis of long- and short-range structures features in titanates Ln2Ti2O7 and zirconates Ln2Zr2O7 (Ln = Gd, Tb, Dy) upon the crystallization process. *J. Phys. and Chem. of Solid*. **130** (2019) 144. https://doi.org/10.1016/j.jpcs.2019.02.019
34. ICDD, International Center for Diffraction Data, http://www.icdd.com
35. R. D. Shannon, C. Prewitt, *T. Acta Cryst.*, **B25** (1976) 925 https://doi.org/10.1107/S0567740869003220
36. P. G. R. Lucuta, F.L. Constantinescu, and D. Barb, Structural Dependence on Sintering Temperature of Lead Zirconate-Titanate Solid Solutions. *J. Am. Ceram. Soc.* **68** (1985) 533. https://doi.org/10.1111/j.1151-2916.1985.tb11519.x

37. P. Naik Pranav, S. Snehal Hasolkar, Consequence of B-site substitution of rare earth (Gd+3) on electrical properties of manganese ferrite nanoparticles. *J. Mater. Sci. Electronics.* **31** (2020) 13434. https://doi.org/10.1007/s10854-020-03897-4

38. R. Chetty, *et al.*, Thermoelectric properties of Co substituted synthetic tetrahedrite. *Acta Mater.* **100** (2015) 266. https://doi.org/10.1016/j.actamat.2015.08.040

39. Y. Li, P. M. Kowalski, G.Beridze, A. R.Birnie, S. Finkeldei, D. Bosbach, Defect formation energies in A2B2O7 pyrochlores. *Scr. Mater.* **107** (2015) 18. https://doi.org/10.1016/j.scriptamat.2015.05.010

40. L. Minervini, R. W. Grimes, K. E. Sickafus, Disorder in Pyrochlore Oxides. *J. Am. Ceram. Soc.* **83** (2000) 1873. https://doi.org/10.1111/j.1151-2916.2000.tb01484.x

41. K. E. Sickafus, *et al.*, Radiation tolerance of complex oxides. *Science* **289** (2000) 748. DOI:10.1126/science.289.5480.748

42. W. Ma, D. E. Mack, R. Vaben, Stöver, D. Perovskite-Type Strontium Zirconate as a New Material for Thermal Barrier Coatings. *J. Am. Ceram. Soc.* **91** (2008) 2630. https://doi.org/10.1111/j.1551-2916.2008.02472.x